

Modeling Inclusion Removal when Using Micro-bubble Swarm in a Full-Scale Tundish with an Impact Pad



SHENG CHANG, ZONGSHU ZOU, BAOKUAN LI, MIHAIELA ISAC,
and RODERICK I.L. GUTHRIE

Gas was injected into the upper part of a water model ladle shroud, producing micro-bubbles by the shearing action of the high-speed entry flow of water, combined with subsequent bubble breaking actions of turbulence. An impact pad was used in favor of a standard turbulence inhibitor, to maintain the integrity of the micro-bubbles, and assure their wide distribution within the tundish. The effects of these two systems on removing small inclusions were investigated, and a numerical model was developed to simulate the motion behaviors of bubbles in the tundish, considering bubble coalescence. Both the turbulence inhibitor and the impact pad performed similar on flow improvement, but the impact pad effectively restrained coalescence between bubbles, leading to a 55.3 pct drop in the average bubble size within the tundish, and generating a 53.9 pct reduction in the residual numbers of inclusions below 51 μm diameter, by contrast with the turbulence inhibitor data. The impact pad fits well with gas bubbling for deep cleaning the liquid steel in tundish.

<https://doi.org/10.1007/s11663-021-02388-z>

© The Minerals, Metals & Materials Society and ASM International 2021

I. INTRODUCTION

LIQUID steel cleanliness is a major concern during continuous casting. The mechanical properties of steel products are highly dependent on the sizes and numbers, of non-metallic inclusions.^[1,2] A typical tundish is the last refractory vessel for holding liquid steel and the most appropriate for removing residual inclusions.^[3–6] This is possible thanks to its typically large volume of steel being handled, under quiescent flow conditions. Many people^[7–11] have modeled the removal of inclusions using various novel flow control devices, such as turbulence inhibitors, weirs, and dams, and these have all proved to be effective in actual steelmaking operations. However, these flow controllers are only efficient

in removing larger inclusions. Inclusions smaller than 50 μm have insufficient buoyancy to de-couple from the liquid steel, their Stokes rising velocities being too low.^[12] They remain within the liquid, entering the Submerged Entry Nozzles (SENs) to the casting machines, and final products.

Inert gas bubbling^[13–15] has been widely employed for cleaning liquid steel. Small inclusions can be attached to the bubble surfaces or captured within the bubble wakes and then be brought to the slag layer by these floating bubbles. Asad *et al.*^[16] reported that carbon monoxide bubbles, formed by decarburizing reactions, can increase the inclusion removal rate by more than 30 pct. Cwudzinski^[17] investigated the hydrodynamic effects of gas injection using porous plugs on liquid steel flows in a one-strand tundish. According to his results, an upward flow of liquid steel formed around the rising bubble column, increased the fraction of active flow in the tundish under both isothermal and non-isothermal conditions. This indirectly promotes the removal of inclusions. Jiang *et al.*^[18] carried out a water modeling study of a four-strand tundish, with a gas curtain located at different positions. They stated that the gas bubbling from the appropriate location can promote uniformity in tundish bath temperatures and in flow characteristics at outlets within a multi-strand tundish. Zhang and Taniguchi^[19] claimed that reducing the bubble size could effectively increase the probability of bubble-inclusion attachment, considering film drainage,

SHENG CHANG is with the Key Laboratory for Ecological Metallurgy of Multimetallic Minerals (Ministry of Education), Northeastern University, Shenyang, 110819, P. R. China and also with the School of Metallurgy, Northeastern University, Shenyang, 110819, P. R. China. Contact e-mail: changs@smm.neu.edu.cn ZONGSHU ZOU is with the Key Laboratory for Ecological Metallurgy of Multimetallic Minerals (Ministry of Education), Northeastern University. Contact e-mail: zouzs@smm.neu.edu.cn BAOKUAN LI is with the School of Metallurgy, Northeastern University. MIHAIELA ISAC and RODERICK I. L. GUTHRIE are with the McGill Metals Processing Centre, McGill University, Montreal, QC, H3A 2B2, Canada.

Manuscript submitted July 25, 2021; accepted November 11, 2021.

Article published online January 8, 2022.

collisions, and sliding, between bubbles and inclusions. In contrast with the behavior of larger bubbles, smaller bubbles have a higher specific surface area, a longer residence time, and a wider distribution within the tundish, all of which are beneficial in the removal of inclusions. Similarly, reducing bubble sizes weaken the impact of rising bubbles at the slag–metal interface,^[20–22] thereby reducing slag droplet entrainment. Unfortunately, conventional bottom gas blowing from a porous plug cannot produce very small bubbles in liquid steel, even for extremely low gas flow rates or small nozzle sizes,^[23] owing to bubble expansion and coalescence at non-wetting interfaces^[24] between liquid steel and a refractory nozzle.

Currently, gas injection into the ladle shroud^[25–28] shows promise as being a potentially effective method for producing micro-bubbles in liquid steel. With this approach, bubbles are separated forcibly from the nozzle by the shearing action of the high entry flow velocities (~ 2 m/s), which inhibits interfacial bubble expansions caused by non-wetting conditions. Once formed and released from the nozzle, these initial bubbles can be further broken down by intense turbulence within the turbulent flow in the ladle shroud, thereby generating even smaller bubbles in liquid steel. According to the measurements by Zhang *et al.*,^[29] a bubble size as small as 1 mm was possible, when gas was injected from the ladle shroud at a flow rate of 0.16 L/min. Chang *et al.*^[30] confirmed that even smaller micro-bubbles could be created, when using gas injection from an injection port close to a partially open-slide gate nozzle, where the local kinetic energy of turbulence is greatest.

The most commonly used flow control to dissipate the downward kinetic energy of the entering stream of steel into the tundish, currently, is to place a turbulence inhibitor immediately below the ladle shroud, in order to protect the tundish bottom from erosion, to decrease the kinetic energy of the entering liquid, and to reverse its direction back up towards the upper surface, so as to prevent short-circuiting flows to the closer exit ports. Nevertheless, the strong mixing of the entry flow within the turbulence inhibitor enhances the coalescence of bubbles and enlarges bubbles within the rising plume. As such, typical turbulence inhibitors are unhelpful in assuring the formation of micro-bubble swarms within a tundish. For this, an impact pad, proposed by McGill Metals Processing Centre (MMPC), was employed to maintain a wide distribution of micro-bubbles, while mirroring the basic functions of typical turbulence inhibitors.

For the present study, physical experiments were carried out in a half-scale model of a commercial four-strand tundish, to investigate the potential for removing very small inclusions ($< 50 \mu\text{m}$), by micro-bubbles generated using the ladle shroud. Hollow glass microspheres (borosilicate glass) were injected into the ladle shroud, corresponding to a size range of equivalent non-metallic inclusions smaller than $102 \mu\text{m}$ in liquid steel. A laser particle scanning analyzer (Mastersizer 2000, Malvern Panalytical Ltd.) was employed to measure the number and size distribution

of inclusions collected at the outlets, and to monitor their removal efficiencies. Similarly, a numerical model was developed to predict the effect of flow controllers on bubble motion behaviors, considering the coalescence of bubbles.

II. PHYSICAL EXPERIMENTS

A half-scale, four-strand water model tundish was established, based on a 12 t capacity industrial prototype, producing 165 mm square billets, operating at a casting speed of 1.5 m/min. Figure 1 shows the configurations of the model tundish and flow controllers with key dimensions. The Reynolds numbers of liquid steel in the prototype and cold water in model tundish were both in the same flow domain, greater than 8000, so that the liquid steel could be replaced by water at room temperature. The modeling process was, therefore, carried out based on equivalent Froude Numbers. The inflow rate was fixed as 30 L/min, being obtained using a 39 pct open slide gate, combined with a bath height of 1.25 m in the ladle. The water flow rate at each of the four outlets was 7.5 L/min, to maintain a 275 mm depth of bath. The ladle shroud with an inner diameter of 23 mm was immersed in the tundish bath to a depth of 30 mm. Similarly, a half-scale impact pad was employed to improve the flow field within the tundish and to maintain a wide dispersion of micro-bubbles. For comparison, water experiments were also carried out in a bare tundish, using a typical turbulence inhibitor.

A novel ladle shroud was developed to produce micro-bubbles by the shearing action of high-velocity entry flow combined with the break-up effects of high turbulence eddies. Inert gas (argon) was injected through laser-drilled ports, as small as 0.2 mm in diameter, located at the upper part of the ladle shroud. Various gas injection schemes can be achieved by controlling gas flow rates, gas injection positions, and numbers of gas ports. For the measurement of bubbles distributed in a 3D space, the scale employed in the post-processing depends on the imaging distance, which impacts the accuracy of bubble measurements. In the present study, bubbles in the entry flow were recorded using a high-speed camera, combined with a high sharpness primary lens being focused on a plane located below the ladle shroud. As such, only the bubbles on this plane could be clearly recorded. This guaranteed the accuracy of the scale for bubble measurement, as other bubbles off this plane were blurred and could be neglected during image post-processing. For each experimental condition, thirty-five photographs of bubble impacts were recorded, taking photo shoots every four seconds.

Non-metallic inclusions were modeled using (hydrophylic) borosilicate glass particles (hollow glass spheres), with a nominal density of 700 kg/m^3 . The particle size ranged from 20 to $120 \mu\text{m}$, corresponding to the non-metallic inclusions in liquid steel with diameter from 17 to $102 \mu\text{m}$, based on the particle similarity criteria proposed by Sahai and Emi.^[31] The particles were completely dispersed in the water by stirring, with a

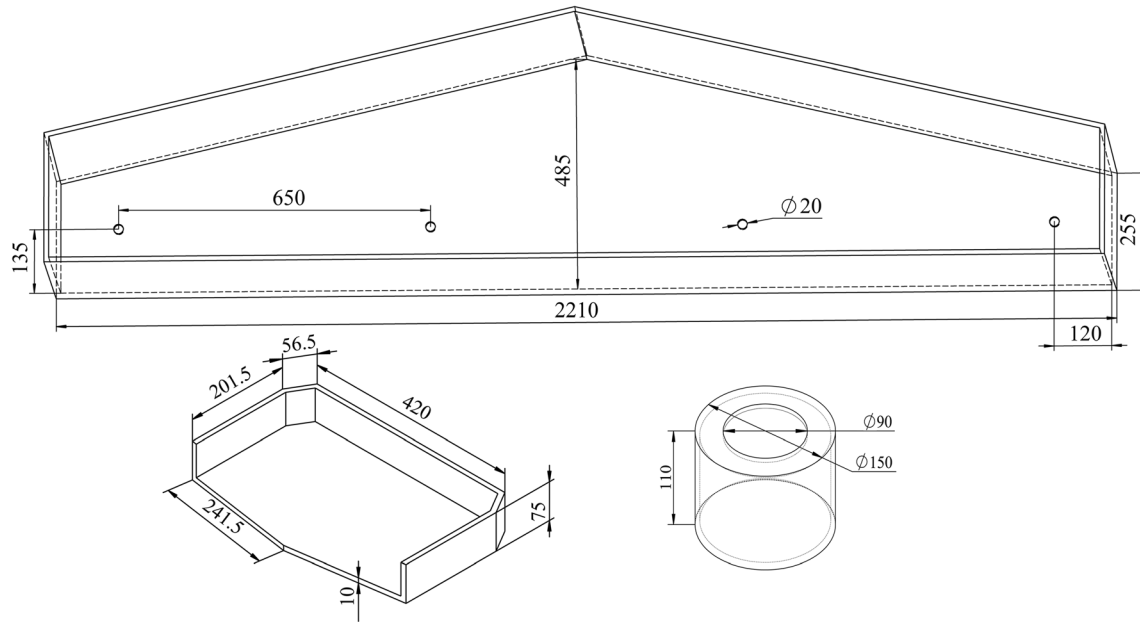


Fig. 1—Configurations of the model tundish and flow controllers with key dimensions (mm).

concentration of 0.4 g/L. To simulate inclusion coming into the real tundish, the particle suspension was continuously injected from the upper part of the ladle shroud at a fixed flow rate of 0.2 L/min. Once the distribution of inclusions within the tundish had reached steady (after two full residence times), inclusions exiting the tundish nozzles were collected, using screen meshes for 10 minutes. Residual inclusions collected at outlets were firstly well dispersed in the solution and hit by parallel laser. The refraction angle of the laser depends on the size of the particle. Therefore, the particle size distribution can be calculated by the laser diffraction pattern. As such, the amount of residual inclusions in each case was calculated by their weight and size distribution.

III. NUMERICAL MODELING

A 3D numerical model was established on the basis of the model tundish, in order to predict the movement and coalescence of bubbles in the tundish with different flow controllers. According to the grid independence test, the computational domain was discretized into 5,600,000 hexahedral grids. The numerical simulation was carried out, based on the following assumptions.

1. The continuous phase (water) was treated as an incompressible Newtonian fluid, of constant density and viscosity.
2. Bubbles were regarded as rigid spheres. The potential for bubble coalescence was considered.

3. The numerical simulations were carried out under the isothermal conditions pertaining to the water model experiments.
4. The top surface of the tundish was assumed to be a flat, free surface, neglecting any fluctuation effects.

A. Governing Equations

The multiphase flow in tundish is simulated by solving a group of governing equations in a 3D Cartesian coordinate system. The continuity equation is given as follows:

$$\frac{\partial \rho}{\partial t} + \frac{\partial(\rho u_i)}{\partial x_i} = 0. \quad [1]$$

Momentum conservation equation can be described as follows:

$$\frac{\partial(\rho u_i)}{\partial t} + \frac{\partial(\rho u_i u_j)}{\partial x_j} = -\frac{\partial P}{\partial x_i} + \frac{\partial}{\partial x_j} \left[\mu_{\text{eff}} \left(\frac{\partial u_i}{\partial x_j} + \frac{\partial u_j}{\partial x_i} \right) \right] + \rho g_i + \vec{f}. \quad [2]$$

The momentum change of continuous phase caused by bubble flotation is considered as a source term. The effective viscosity (μ_{eff}) can be calculated as the sum of the laminar viscosity and turbulent viscosity, kg/m-s.

$$\mu_{\text{eff}} = \mu + \mu_t. \quad [3]$$

The transport equations for turbulence kinetic energy (k) and its dissipation rate (ϵ) are given by

$$\frac{\partial(\rho k)}{\partial t} + \frac{\partial(\rho u_j k)}{\partial x_j} = \frac{\partial}{\partial x_j} \left[\left(\mu + \frac{\mu_t}{\sigma_k} \right) \frac{\partial k}{\partial x_j} \right] + G_k - \rho \varepsilon, \quad [4]$$

$$\begin{aligned} \frac{\partial(\rho \varepsilon)}{\partial t} + \frac{\partial(\rho u_j \varepsilon)}{\partial x_j} = & \frac{\partial}{\partial x_j} \left[\left(\mu + \frac{\mu_t}{\sigma_\varepsilon} \right) \frac{\partial \varepsilon}{\partial x_j} \right] + \rho C_1 S \varepsilon \\ & - \rho C_2 \frac{\varepsilon^2}{k + \sqrt{v \varepsilon}}. \end{aligned} \quad [5]$$

The model parameter, C_1 , is given by a max function.

$$C_1 = \max \left[0.43, \frac{\eta}{\eta + 5} \right]. \quad [6]$$

The generation rate of turbulent kinetic energy caused by mean velocity gradients, G_k , can be calculated as follows:

$$G_k = \mu_t \frac{\partial u_j}{\partial x_i} \left(\frac{\partial u_i}{\partial x_j} + \frac{\partial u_j}{\partial x_i} \right). \quad [7]$$

The turbulent viscosity, μ_t , can be calculated as follows:

$$\mu_t = C_\mu \rho \frac{k^2}{\varepsilon}, \quad [8]$$

where C_μ is a variable, which can be described as a function of k and ε . The model constants are assigned as follows: $C_2 = 1.9$, $\sigma_k = 1.0$, and $\sigma_\varepsilon = 1.2$.^[32]

B. Discrete Phase Model

The trajectory of each bubble was calculated by integrating the force balance equation in an Euler-Lagrangian frame. The forces on each bubble are obtained from the local continuous phase flow in the previous time step.

$$\frac{du_b}{dt} = \frac{3\mu C_D Re}{4\rho_g d_b^2} (u - u_b) + \frac{g(\rho_g - \rho)}{\rho_g} + F_m + F_p + F_l. \quad [9]$$

The accelerations on the bubble caused by drag force and buoyancy force are listed as the first two terms of the equation. The drag coefficient can be calculated as a function of Reynolds number, assuming that bubbles are spherical.

$$C_D = a_1 + \frac{a_2}{Re} + \frac{a_3}{Re}, \quad [10]$$

where a_1 , a_2 , and a_3 are model constants, and those can be assigned according to the range of Reynolds number.

The effects of virtual mass force (F_m), pressure gradient force (F_p), and lift force (F_l) on bubble movement are also taken into consideration.

$$F_m = C_{VM} \frac{\rho}{\rho_g} \left(u_b \nabla u - \frac{du_b}{dt} \right), \quad [11]$$

$$F_p = \left(\frac{\rho}{\rho_g} \right) u_b \nabla u, \quad [12]$$

$$F_L = C_L \frac{\rho}{\rho_g} (u - u_b) (\nabla \times u), \quad [13]$$

where C_{VM} represents the virtual mass factor, being assigned a value of 0.5; C_L is the lift coefficient with a value of 0.1.^[33] The discrete random walk model was employed to predict the dispersion of bubbles due to turbulence within the liquid flow. The momentum change of each bubble was returned to the source term in the momentum conservation equation, to re-calculate the liquid flow at the next time step. This achieves the two-way coupling between the discrete and continuous phases.

$$F = \sum \left[-\frac{3\mu C_D Re}{4\rho_g d_b^2} (u - u_b) + F_{\text{other}} \right] \dot{m}_b \Delta t, \quad [14]$$

where \dot{m}_b is the mass flow rate of bubbles, kg/s; Δt represents the time step of bubble injection, 0.001s, considering the actual amount of bubbles coming into the tundish bath.

C. Coalescence Model

The collision and coalescence of bubbles described by the O'Rourke's algorithm^[34] were applied for treating interactions between bubbles. A collision probability between two bubbles can be calculated, according to

$$P = \frac{\pi(r_1 + r_2)^2 u_{\text{rel}} \Delta t}{V_{\text{cell}}}, \quad [15]$$

where V_{cell} is the volume of the cell, m^3 ; u_{rel} denotes the relative velocity between two bubbles; $\pi(r_1 + r_2)u_{\text{rel}}\Delta t$ represents the collision volume, m^3 , which is the swept volume of collision area in a time step. In general, bubbles tend to coalesce following head-on collisions and tend to bounce off each other, with an oblique collision. For a pair of colliding bubbles, their coalescence probability depends on the critical offset of their collision.

$$b_{\text{crit}} = (r_1 + r_2) \sqrt{\min \left(1.0, \frac{2.4f}{We} \right)}, \quad [16]$$

where f can be defined as a function of r_1/r_2 .

$$f(r_1/r_2) = (r_1/r_2)^3 - 2.4(r_1/r_2)^2 + 2.7(r_1/r_2), \quad [17]$$

We is the collision Weber number.

$$We = \frac{\rho u_{\text{rel}}^2 d_m}{\sigma}, \quad [18]$$

where u_{rel} is the relative velocity between two bubbles, m/s; d_m represents the mean diameter of two bubbles, m; σ is the interfacial tension between bubbles and liquid, being assigned as 0.072 N/m. The actual collision parameter is given by

$$b = (r_1 + r_2)\sqrt{Y}, \quad [19]$$

where Y represents a random number between 0 and 1.^[35] If the actual collision parameter is smaller than the critical offset, two colliding bubbles can coalesce into a larger one. The properties of the coalesced bubble follow the basic conservation laws. Otherwise, the bubble collision is judged as a grazing collision, without any bubble mass change. The bubble's velocity updates on the basis of the momentum conservation and kinetic energy conservation. In O'Rourke's algorithm, the bubbles are replaced by bubble parcels, to reduce the computational cost of the bubble collisions to a reasonable level.

D. Boundary Conditions and Solution Procedures

The computational work was carried out using the CFD software ANSYS Fluent 18.0, based on the finite volume method. A velocity inlet was employed for the injection of the continuous phase, with an entry flow velocity of 1.8 m/s. The initial turbulent intensity and turbulent length scale are assigned 0.039 and 0.0031 m, calculated by the entry flow velocity and dimension of the ladle shroud. The submerged entry nozzles are set as pressure outlets at zero gage pressure. All the solid walls were treated as stationary, no-slip boundaries. The standard wall function was employed to calculate movement of the near-wall flows. The pressure-velocity coupling is achieved using the Semi-Implicit Method for Pressure-Linked Equations Consistent algorithm. The calculation regards one has achieving convergence, once the normalized residuals of all terms are less than 10^{-4} , within a time step of 0.0005 second.

IV. RESULTS AND DISCUSSION

A. RTD Analysis

The residence time distribution (RTD) of the liquid flow in tundish was measured by the stimulus-responding method. A certain amount of tracer was injected into the ladle shroud within 2 seconds. The probe was employed to detect the conductivity of liquid flowing out of each strand, to obtain the RTD curve for the data acquisition system. Owing to the symmetry of the model structure, only two strands located on one side of the tundish were considered in the RTD analysis. The combined model was employed to calculate the flow characteristics, such as the volume fractions of dead region (V_d/V), plug flow (V_p/V), and well-mixed flow (V_m/V).

$$\frac{V_d}{V} = 1 - \frac{Q_a}{Q}\bar{\theta}_c, \quad [20]$$

$$\frac{V_p}{V} = \frac{\theta_{\min} + \theta_{\max}}{2}, \quad [21]$$

$$\frac{V_m}{V} = 1 - \frac{V_d}{V} - \frac{V_p}{V}, \quad [22]$$

where $\bar{\theta}_c$ is the dimensionless mean residence time, θ_{\min} and θ_{\max} represent the dimensionless responds time and peak time; Q_a/Q is the fraction of active flow rate, which can be calculated as the area under RTD curve in a dimensionless time of 0 to 2. The flow characteristics of the entire tundish can be calculated as the average of those at inner strand and outer strand, due to their same flow rates.

As shown in Figure 2, the two RTD curves for the bare tundish are similar to those in a bare tundish with gas bubbling. The dead volume fraction of the inner strand is up to 39.7 pct in the bare tundish. A short-out flow exists between the ladle shroud and the inner nozzle, reducing its average residence time. As the outer nozzle is far from the ladle shroud, the flow characteristic at outer strand is better than that at inner strand. The bubble flotation has rare impact on the liquid flow of the tundish, due to the small sizes of bubbles. The difference in dead volume fraction between the tundish with and without small bubbles is as less as 0.4 pct.

Figure 3 displays a typical picture of bubbles coming out of the novel ladle shroud, produced by gas injection through four ports at a gas flow rate of 0.2 L/min. Owing to the shearing action of the entry flow combined with the bubble break-up effects of the turbulence, most of the bubbles concentrate in the size bins smaller than 1 mm. The mean size of the bubbles is 0.81 mm, according to the post-processing of 35 photos. In contrast with the bubbles produced by the conventional gas curtain technique, the bubbles generated by gas injection within the ladle shroud are much smaller. They are more widely distributed within the liquid and do not generate a significant upward flow of liquid around them.

However, in the tundish with a conventional turbulence inhibitor, the liquid from ladle shroud is well mixed in a small pot or chamber. This effectively dissipates the turbulence kinetic energy of the entry flow. The entry flow reverses through the edges of the turbulence inhibitor, moving upward to the liquid surface. As shown in Figure 4, the turbulence inhibitor effectively eliminates the short-cut flows to the inner strands (SEN's) and improves the flow field within the entire tundish. Owing to the flow improvement by the turbulence inhibitor, the entire dead volume fraction of the tundish is reduced from 37.0 to 27.7 pct. Indeed, the main function of the turbulence inhibitor is to smooth the fluid flow outside of the pouring region, providing a stable dynamic condition for the flotation of large

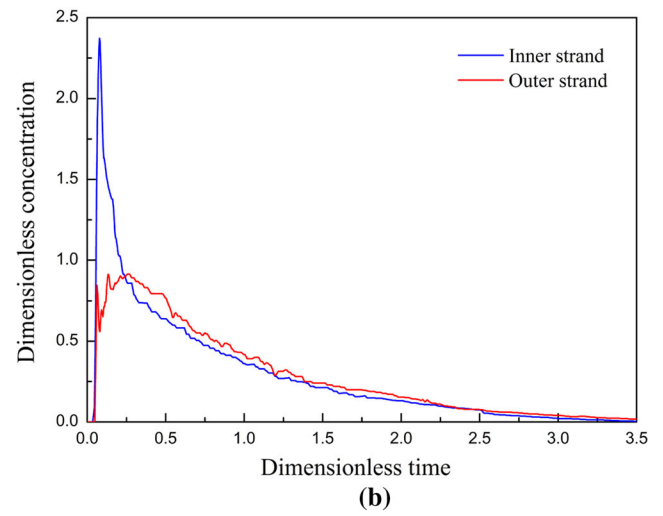
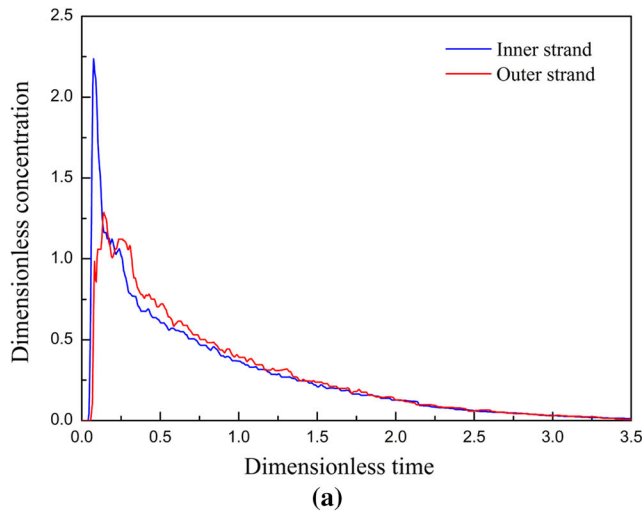


Fig. 2—Experimental residence time distributions of the liquid in (a) a bare tundish, (b) a bare tundish with gas bubbling.

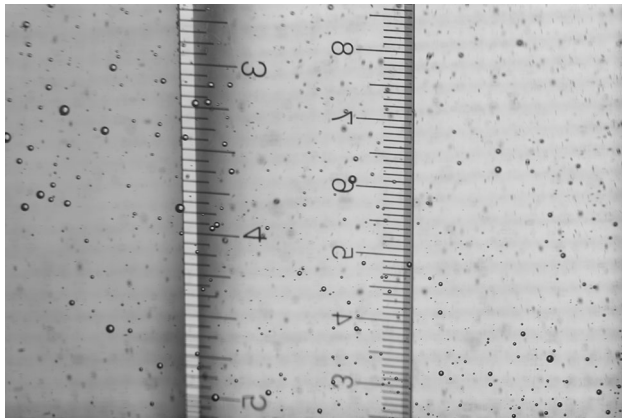


Fig. 3—Typical photo of bubbles generated by four-port gas injection at fixed gas flow rate of 0.2L/min.

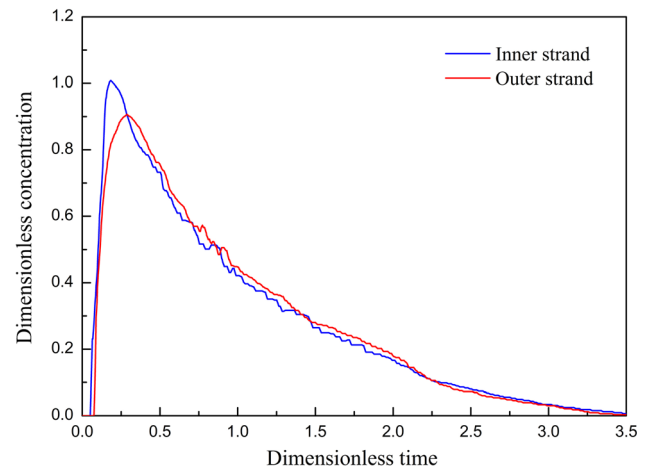


Fig. 5—Residence time distributions of liquid in the tundish with the impact pad and gas bubbling.

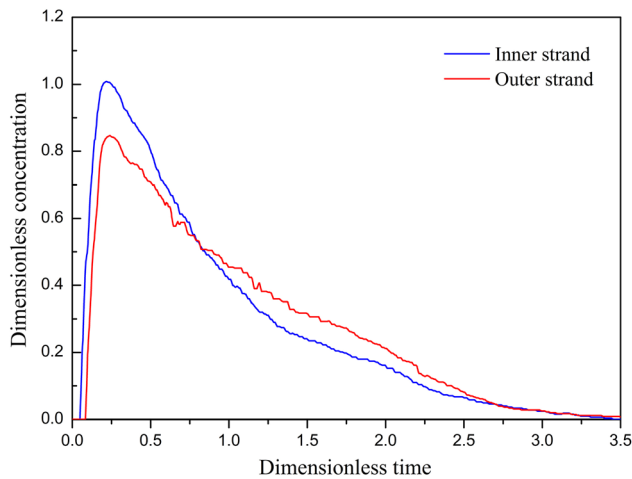


Fig. 4—Residence time distributions of liquid in the tundish with the turbulence inhibitor and gas bubbling.

inclusions. Nevertheless, the well-mixed flow in such a small space significantly enhances bubble coalescence, leading to the elimination of micro-bubbles through

coalescence and growth. As such, the turbulence inhibitor is not applicable to a tundish employing micro-bubbles.

Given this, the impact pad was favored for these conditions. Figure 5 shows the RTD curves in the tundish using this impact pad with gas bubbling. The entry flow reverses along the side wall of the impact pad after hitting the pad bottom, forming a similar upward flow. According to the RTD analysis, the volume fraction of dead region in the tundish with impact pad is as small as 28.4 pct, similar to a conventional turbulence inhibitor. Besides, the plug volume and mixing volume are quite similar for the two tundish configurations, with a relative error of less than 1 pct.

B. Bubble Motion Behaviors

The effects of the two flow controllers on bubble coalescence were predicted by numerical simulation. The initial diameter of bubbles flowing out of the ladle shroud was assigned as being 0.8 mm, corresponding to

the average size of bubbles coming from the ladle shroud in the water experiment. As shown in Figure 6, the entry flow is well mixed in the chamber of the turbulence inhibitor, leading to the intensive bubble coalescence. Then, the incoming jet flow is reversed back to the top surface through the port of the turbulence inhibitor. The predicted distribution of bubbles in the tundish with the turbulence inhibitor is shown in Figure 7. Bubbles gather within the small space following with this vertical reverse flow, which enhances the coalescence of existing micro-bubbles, leading to bubble growth. The mean bubble size was increased by 0.38 mm, from 0.8 to 1.18 mm, due to the intensive bubble coalescence in the tundish with turbulence inhibitor. Besides, some bubbles can be trapped by large eddies in the semi-closed chamber formed by

turbulence inhibitor, with its overhanging lips, or eaves. This causes the bubbles to collide, over and over again. Maximum bubble sizes up to 5.90 mm are predicted. This clearly indicates a strong bubble impact on the slag layer.

In the tundish with an impact pad, micro-bubbles can spread widely in the liquid bath (as shown in Figure 8), forming a large bubble swarm. The collision probability of bubbles is decreased owing to the reduction in bubble number density. The mean bubble size was only increased by 0.17 mm, which is 55.3 pct smaller than that in the tundish with the turbulence inhibitor. There is no significant eddy formation in the impact pad; therefore, all bubbles can move upward with the reversed flow. This avoids the formation of the extremely large bubble sizes caused by major

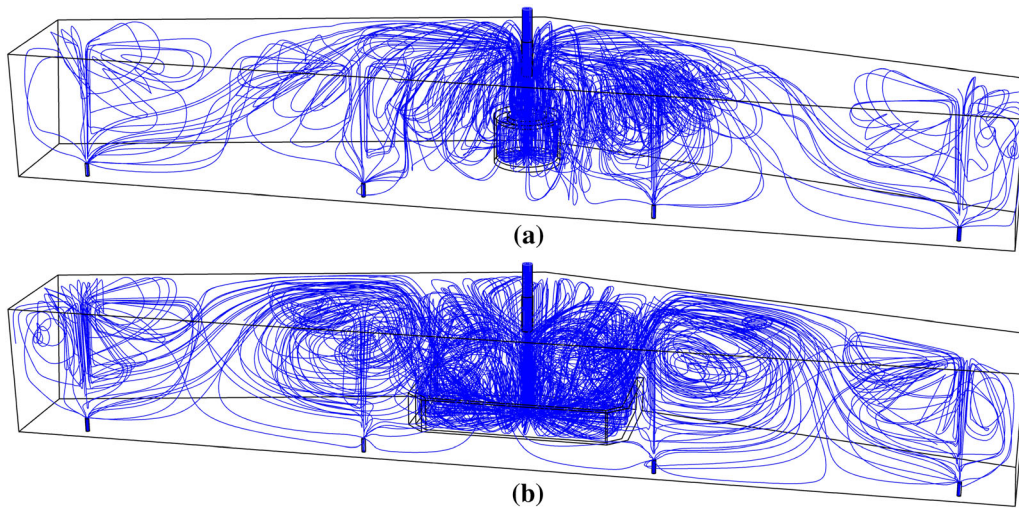


Fig. 6—Flow path line in the tundishes with (a) turbulence inhibitor, (b) impact pad.

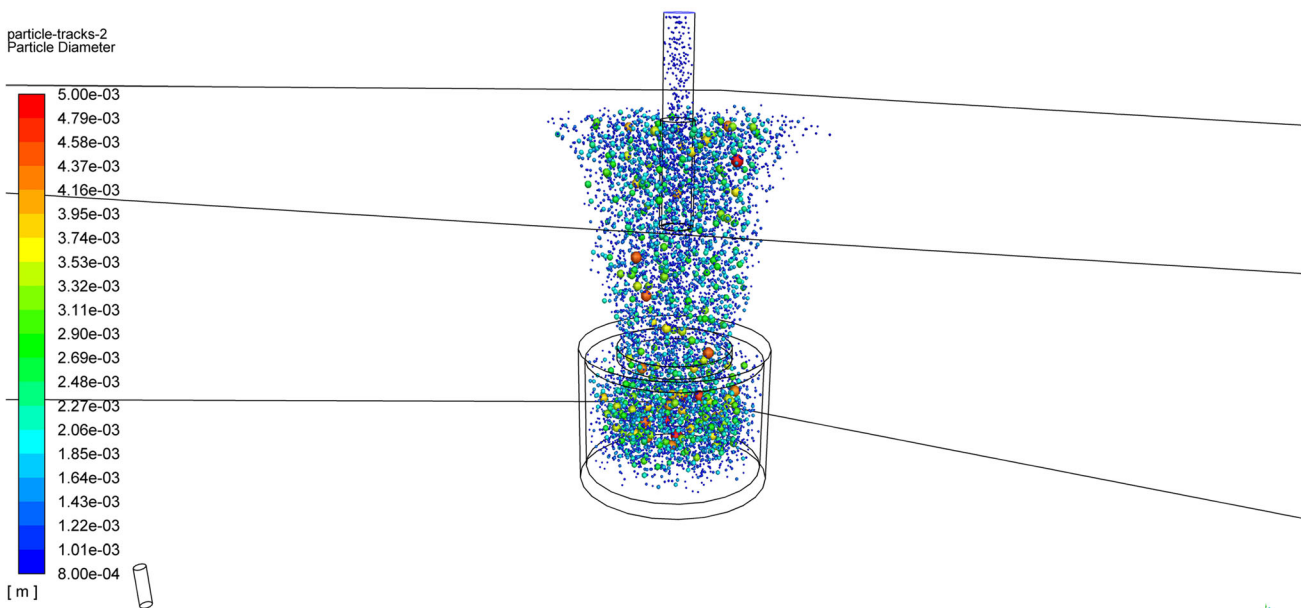


Fig. 7—Predicted bubble distribution in the tundish with turbulence inhibitor.

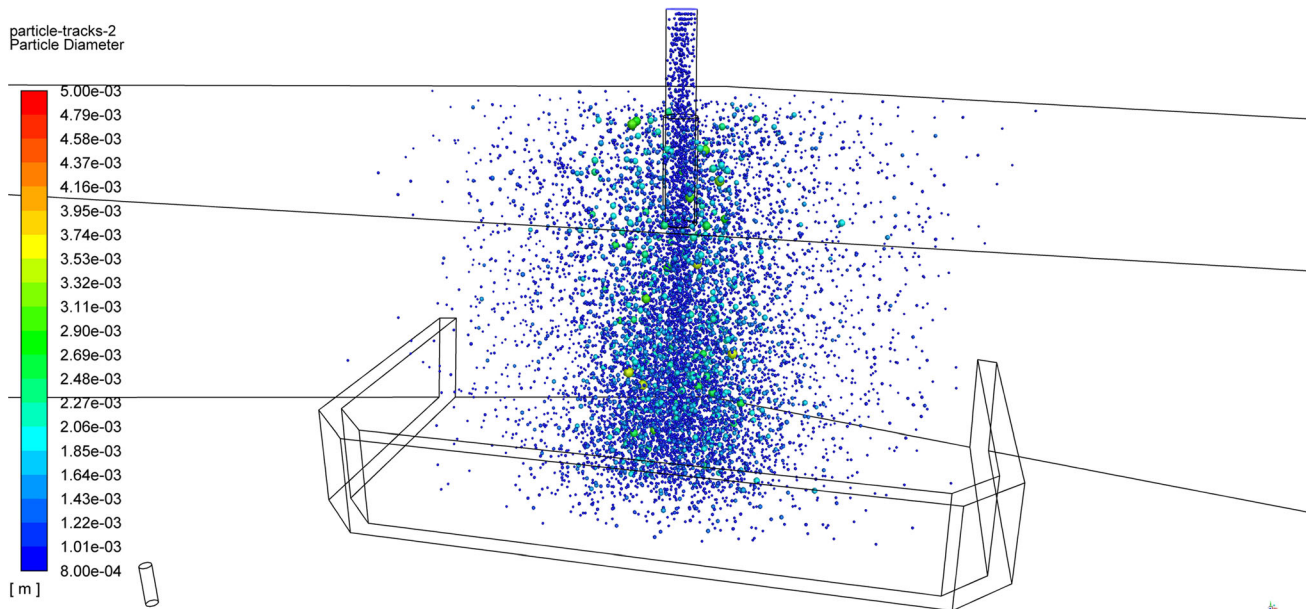


Fig. 8—Predicted bubble distribution in the tundish with impact pad.

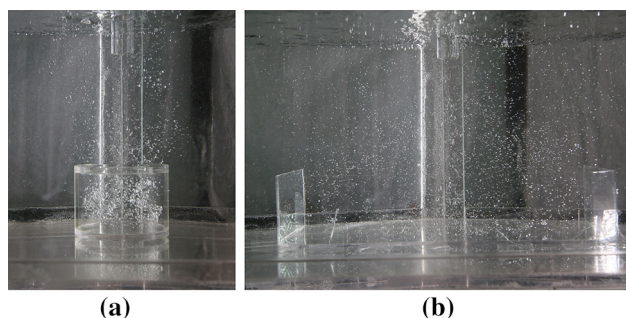


Fig. 9—Bubble distributions in the tundish with (a) turbulence inhibitor, (b) impact pad.

coalescence phenomena. As shown in Figure 9, the predicted bubble distributions were in good agreement with those obtained in physical model.

Figure 10 shows the size distribution of bubbles obtained by post-processing of numerical simulation. In the tundish with the impact pad, 59.1 pct of the bubbles can remain independent during flotation and 14.8 pct of the bubbles are larger than 1.27 mm, and these have coalesced only two times. Most bubbles are kept in small sizes. In the tundish with the turbulence inhibitor, only 38.9 pct of the entry bubbles flow up to the top surface without coalescence. More than 29.4 pct of the bubbles were larger than 1.27 mm, due to the strong bubble coalescence. This weakens the effectiveness of bubbles on inclusion removal.

C. Detection of the Input Inclusions

Inclusions were well mixed in water by stirring paddle, forming an inclusion suspension. When the liquid flow field reached stable, inclusion suspension was continuously injected into the upper part of the ladle shroud. A fixed

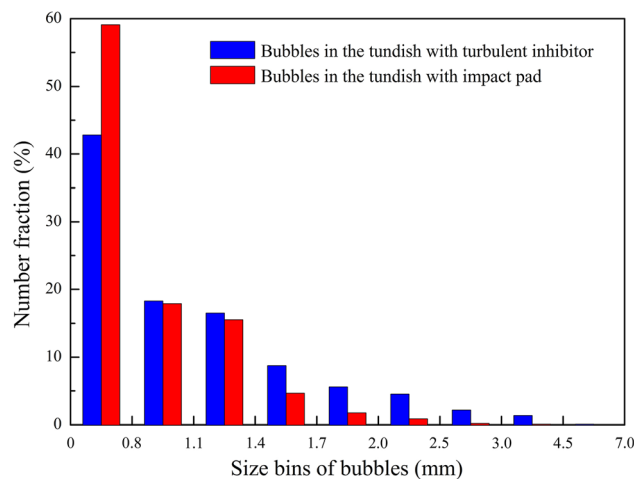


Fig. 10—Size distributions of bubbles in the thundish with different flow controllers.

flow rate (0.2 L/min) of the inclusion suspension was maintained by a low speed peristaltic pump. The initial size distribution of inclusions used in water modeling was obtained by sizing analysis. As shown in Figure 11, most of the inclusions are located within the size intervals smaller than 58.65 μm . The weight of inclusions in each size bin approximately fits a normal distribution.

Given the size distribution of inclusions introduced into the tundish, the total number of inclusions can be calculated as follows:

$$N_p = \frac{m_p}{\rho_p \sum P_i \frac{1}{6} \pi d_i^3}, \quad [23]$$

where m_p represents the particle mass, kg; d_i is the average diameter of particles in a size bin, m; P_i is proportion of the particles in the corresponding size bin,

–. As such, the inclusion number density of inlet liquid can be given by

$$n_i = \frac{N_p Q_s}{V_s Q_i} = 170000/L, \quad [24]$$

where V_s is the total volume of the suspension, L; Q_s and Q_i represent the flow rates of the suspension and inlet liquid, respectively, L/min.

After the inclusion distribution reaching stable, screen cloth with high mesh number was employed to collect the inclusions coming out of the tundish nozzle those would potentially remain in the casting slab during the operation process of the mold. These inclusions were dried, weighed, and measured by grading analysis. The number of the residual inclusions in a time slot can be obtained based on their weight and size distribution. The inclusion residual rate is defined as the proportion of the outflow inclusions number density to the inflow inclusion number density.

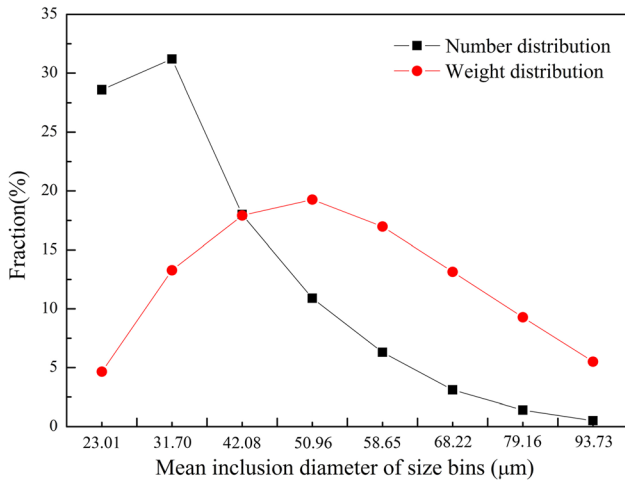


Fig. 11—Number and weight distribution of inclusions in the entry flow.

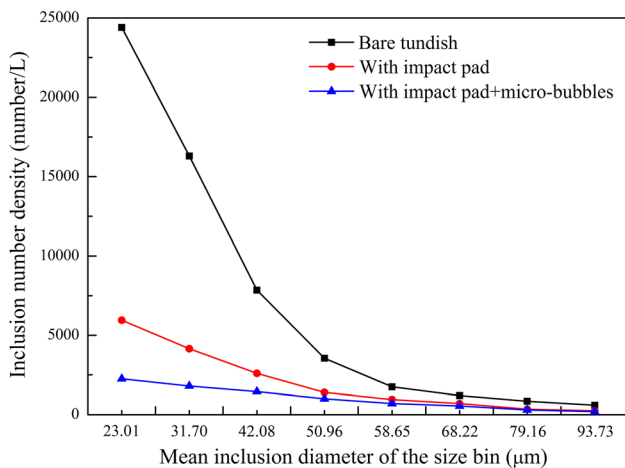


Fig. 12—Size distributions of residual inclusions in different cases.

D. Inclusion Removal

Inclusion number density of each case is listed in Table I. The inclusion removal rate of the bare tundish is as high as 66.7 pct, owing to the large volume of the tundish. The inclusion number density of the liquid at inner nozzle is up to 73200/L, which is 83.5 pct higher than that of the liquid at the outer nozzle. As the inner nozzle is closer to the ladle shroud, the entry flow would move directly to the inner nozzle in the bare tundish, forming a short-circuit flow. The inclusions are easy to flow out through the inner nozzle following with the liquid path lines. By contrast, the outer strand is far from the ladle shroud with a longer residence time. Inclusions have sufficient time to float up, so that inclusion number density at outer nozzle is lower. The distribution of inclusion number density at each nozzle is in accordance with the RTD analysis.

In the bare tundish with gas bubbling, the inclusion number density of the entire outflow was reduced from 56550 to 38200/L, a drop of 32.5 pct. It is noteworthy that the removal of inclusion by bubble flotation is almost irrelevant to the changes in flow characteristics. These small bubbles with such a large distribution are insufficient to drive a significant upward flow, so that they have little impact on the flow field of the tundish. This is also validated by the corresponding RTD analysis. Therefore, the inclusion removal by small bubbles is mainly due to the effect of their attachment to micro-bubble surfaces, rather than flow optimization by floating bubbles.

In Case 3, the entry flow first hits the pad's bottom, then reverses along the sidewalls of the impact pad, forming an upward flow. Inclusions can move to the tundish surface following with the upward flow and then be absorbed by the top slag. Besides, the eaves of the impact pad eliminate the short-out flow from ladle shroud to inner nozzle, increasing the residence time of the inner strand. With an impact pad, the inclusion number density of the entire outflow is decreased from 56550 to 16350/L, dropped by 71.1 pct. Compared with gas bubbling, the flow controller shows a more direct improvement on inclusion removal. However, it is unrealistic to employ plenty flow controllers to deeply clean the liquid steel in tundish, considering the refractory erosion and active volume occupation by flow controllers. Besides, the effect of flow improvement on the removal of small inclusions is limited. When using gas bubbling combined with an impact pad, the inclusion number density of the entire outflow can be further reduced to 8250/L, with a significant drop of 49.5 pct. As 90.4 pct of the inclusions has already been removed in the tundish with the impact pad, such a great amount of inclusion removal caused by gas bubbling on that basis can be regarded as a significant promotion on the cleanliness of liquid steel.

Compared with the tundish with an impact, the tundish with a turbulence inhibitor has a slightly longer residence time, according to the RTD analysis. As expected, the turbulence inhibitor also performs better than the impact pad on inclusion removal, leading to a 7.3 pct reduction of the inclusion number density of the

Table I. Inclusion Number Density of Liquid Flow in Different Cases (Number/L)

	Inner Nozzles	Outer Nozzles	Overall	Removal Rate (Pct)
Entry Flow	—	—	170000	—
Case 1 (Bare Tundish)	73200	39900	56550	66.7
Case 2 (Bare Tundish + Bubbles)	50500	25900	38200	77.5
Case 3 (Tundish with IP)	21200	11500	16350	90.4
Case 4 (Tundish with IP + Bubbles)	10800	5700	8250	95.1
Case 5 (Tundish with TI)	20300	10000	15150	91.1
Case 6 (Tundish with TI + Bubbles)	18900	8800	13850	91.9

entire outflow. In essence, the turbulence inhibitor and impact pad remove inclusions by the same approach, producing the upward flow. However, the combination of gas bubbling and a turbulence inhibitor cannot live up to expectations on cleaning liquid steel. The inclusion number density of the entire outflow is 13850/L, which is 67.9 pct higher than that in the tundish with gas bubbling and an impact pad. This goes against to the prediction of RTD analysis. The intense mixing flow in the turbulence inhibitor enhances the bubble coalescence, leading to the grow-up of existing small bubbles following with the entry flow. Therefore, the effect of small bubbles on inclusion removal is severely weakened and only leads to a 0.8 pct promotion of the inclusion removal rate. By contrast with turbulence inhibitor, impact pad is a more appropriate flow controller for the tundish with gas bubbling from ladle shroud.

The size distributions of the residual inclusions collected in water experiments are shown in Figure 12. In the bare tundish, 77.1 pct of the inclusions larger than $51\mu\text{m}$ can float up to the top surface by their buoyancy. With the impact pad, the number density of large inclusions ($> 51\mu\text{m}$) and smaller inclusions ($< 51\mu\text{m}$) are decreased by 72.9 and 48.9 pct, respectively. The upward flow produced by the impact pad is effective on the removal of both large inclusions and small inclusions. When combined gas bubbling with the impact pad, the number density of smaller inclusions is further reduced by 53.9 pct. By contrast, the removal rate of large inclusions changes rarely, only with a drop of 22.2 pct. Basically, the removal of large inclusions depends on the capture of bubble wakes. As most of the bubbles in the present study are smaller than 2 mm, their weak flows are insufficient to capture large inclusions. The floating small bubble is mainly effective on the removal of small inclusions. Therefore, gas bubble can be regarded as an advanced method for deep cleaning the liquid steel, based on the premise that most of large inclusions have already been removed by conventional flow controllers.

V. CONCLUSIONS

In the present study, physical experiments were carried out to investigate inclusion removal by micro-bubble swarms in a delta shape, four-strand tundish. The impact pad was employed as a replacement to the turbulence Inhibitor, to maintain a wide bubble

distribution within the tundish. The difference in dead volume between the tundishes using two flow controllers is less than 0.7 pct, indicating that the impact pad also performs well for flow optimization.

A numerical model based on the Euler–Lagrangian approach was developed to simulate the bubble behaviors in the tundish with different flow controllers, considering the coalescence between bubbles. The model predictions show that the average bubble size is increased by 0.27 mm in the tundish with a turbulence inhibitor, due to intensive bubble coalescence. By contrast, the impact pad effectively inhibits the coalescence of micro-bubbles by providing a widely distributed array of bubbles, only leading to a 0.17 mm increase of the average bubble size. This is beneficial in maintaining smaller sized bubbles for inclusion removal. The inclusion detection indicates that most of the inclusions can be removed by impact pad. The micro-bubbles can further promote the removal of inclusions smaller than $51\mu\text{m}$, leading to another 53.9 pct reduction of residual inclusions. Compared with the turbulence inhibitor, the impact pad is more suitable to cooperate with gas bubbling for deep cleaning the liquid steel in the tundish.

ACKNOWLEDGMENTS

The present work was supported by the National Natural Science Foundation of China (51904061).

CONFLICT OF INTEREST

The authors declare that they have no conflict of interest

ABBREVIATIONS

C_D	Drag coefficient (–)
C_{VM}	Virtual mass factor (–)
C_L	Lift coefficient (–)
d_b	Diameter of bubble (m)
g	Gravity acceleration (m^2/s)
G_k	Generation rate of turbulence kinetic energy (–)
k	Turbulent kinetic energy (m^2/s^2)

\dot{m}_b	Dimensionless mean residence time (–)
m_p	Mass of particles (kg)
n_i	Number density of inclusions (number/m ³)
N_p	Total number of inclusions (–)
P	Pressure (Pa)
Q_a	Active flow rate (m ³ /s)
Q_i	Inlet flow rate (m ³ /s)
Q_s	Volume flow rate of inclusion suspension (m ³ /s)
Re	Reynolds number (–)
r_1, r_2	Radius of two colliding bubbles (m)
Δt	Time step (s)
u, u_b	Velocity of fluid flow and bubbles (m/s)
u_{rel}	Relative velocity between two colliding bubbles (m/s)
V_{cell}	Volume of the cell (m ³)
V_s	Volume of inclusion suspension (m ³)
We	Weber number (–)
ρ, ρ_g, ρ_p	Densities of liquid, gas, and particle (kg/m ³)
ε	Turbulent dissipation rate (m ² /s ³)
$\bar{\theta}_c$	Dimensionless mean residence time (–)
$\theta_{min}, \theta_{max}$	Dimensionless responds time and peak time (–)
σ_ε	Turbulent Prandtl number for turbulent dissipation rate (–)
μ_{eff}, μ, μ_t	Effective viscosity, laminar viscosity, and turbulent viscosity (kg/m-s)
RTD	Residence time distribution
SEN	Submerged Entry Nozzle

REFERENCES

- S. Tokuda, I. Muto, Y. Sugawara, and N. Hara: *Corros. Sci.*, 2020, vol. 167, p. 108506.
- D. Tang and P.C. Pistorius: *Metall. Mater. Trans. B*, 2021, vol. 52B, pp. 580–85.
- K. Chattopadhyay, R.I.L. Guthrie, and M. Isac: *ISIJ Int.*, 2010, vol. 50, pp. 331–48.
- S. Chang, X.K. Cao, C.H. Hsin, Z.S. Zou, M. Isac, and R.I.L. Guthrie: *ISIJ Int.*, 2016, vol. 56, pp. 1188–97.
- D. Mazumdar: *Metall. Mater. Trans. B*, 2021, vol. 52B, pp. 23–29.
- J.H. Park and L.F. Zhang: *Metall. Mater. Trans. B*, 2020, vol. 51B, pp. 2453–82.
- A. Cwudzinski: *Steel Res. Int.*, 2015, vol. 86, pp. 972–83.
- J.S. Zhang, Q. Liu, S.F. Yang, Z.X. Cheng, J.S. Li, and Z.Y. Jiang: *ISIJ Int.*, 2019, vol. 59, pp. 1167–77.
- S.K. Ray, M. Isac, and R.I.L. Guthrie: *Ironmak. Steelmak.*, 2011, vol. 38, pp. 173–80.
- M.R.M. Yazdi, A.R.F. Khorasani, and S. Talebi: *Can. Metall. Q.*, 2019, vol. 58, pp. 379–88.
- P.Y. Ni, L.T.I. Jonsson, M. Ersson, and P.G. Jonsson: *Steel Res. Int.*, 2016, vol. 87, pp. 1356–65.
- S. Lopez-Ramirez, J. D. J. Barreto, Palafox-Ramos, R. D. Morales and D. Zacharias: *Metall. Mater. Trans. B* 2001, vol. 32B, pp. 615–27.
- H.J. Yang, S. Vanka, and B.G. Thomas: *JOM*, 2018, vol. 70, pp. 2148–56.
- S. Chang, L.C. Zhong, and Z.Z. Zou: *ISIJ Int.*, 2015, vol. 55, pp. 837–44.
- S. Chang, X.K. Cao, Z.S. Zou, M. Isac, and R.I.L. Guthrie: *Metall. Mater. Trans. B*, 2016, vol. 47B, pp. 2732–43.
- A. Asad, M. Haustein, K. Chattopadhyay, C.G. Aneziris, and R. Schwarze: *JOM*, 2018, vol. 70, pp. 2927–33.
- A. Cwudzinski: *Ironmak. Steelmak.*, 2018, vol. 45, pp. 528–36.
- J. Jiang, J.S. Li, H.J. Wu, S.F. Yang, T. Li, and H.Y. Tang: *Int. J. Miner. Metall. Mater.*, 2010, vol. 17, pp. 143–48.
- L.F. Zhang and S. Taniguchi: *Int. Mater. Rev.*, 2000, vol. 45, pp. 59–82.
- S. Chang, Z.S. Zou, J.H. Liu, M. Isac, X.K.E. Cao, X.F. Su, and R.I.L. Guthrie: *Powder Technol.*, 2021, vol. 387, pp. 125–35.
- S. Chatterjee and K. Chattopadhyay: *ISIJ Int.*, 2015, vol. 55, pp. 1416–24.
- S. Chatterjee, D.H. Li, and K. Chattopadhyay: *Metall. Mater. Trans. B*, 2018, vol. 49B, pp. 756–66.
- S. Chang, X.K. Cao, Z.S. Zou, M. Isac, and R.I.L. Guthrie: *ISIJ Int.*, 2018, vol. 58, pp. 60–67.
- D. Gerlach, G. Biswas, F. Durst, and V. Kolobaric: *Int. J. Heat Mass Transfer*, 2005, vol. 48, pp. 425–38.
- S. Chang, W.X. Huang, Z.Z. Zou, B.K. Li, and R.I.L. Guthrie: *Powder Technol.*, 2020, vol. 367, pp. 296–304.
- P.K. Singh and D. Mazumdar: *Metall. Mater. Trans. B*, 2019, vol. 50B, pp. 1091–1103.
- Y. Li, C.G. Cheng, M.L. Yang, Z.X. Dong, and Z.L. Xue: *Metals*, 2018, vol. 8, p. 590.
- R. Liu and B.G. Thomas: *Metall. Mater. Trans. B*, 2015, vol. 46B, pp. 388–405.
- Q.Y. Zhang, L.T. Wang, and Z.R. Xi: *ISIJ Int.*, 2006, vol. 8, pp. 1177–82.
- S. Chang, X.K. Cao, and Z.Z. Zou: *Metall. Mater. Trans. B*, 2018, vol. 49B, pp. 953–57.
- Y. Sahai and T. Emi: *ISIJ Int.*, 1996, vol. 36, pp. 1166–73.
- C. Laborde-Boulet, F. Larachi, N. Dromard, O. Delsart, and D. Schweich: *Chem. Eng. Sci.*, 2009, vol. 64, pp. 4399–4413.
- A. Tomiyama, H. Tamai, I. Zun, and S. Hosokawa: *Chem. Eng. Sci.*, 2002, vol. 57, pp. 1849–58.
- P. J. O'Rourke: *Ph.D Thesis*, Princeton University, Princeton, New Jersey, 1981.
- M. Mezhericher, A. Levy, and I. Borde: *Int. J. Multiphase Flow*, 2012, vol. 43, pp. 22–38.

Publisher's Note Springer Nature remains neutral with regard to jurisdictional claims in published maps and institutional affiliations.